

Article

Effect of Water-Soluble Chlorine-Containing Buckminsterfullerene Derivative on the Metabolism of Reactive Oxygen Species in Human Embryonic Lung Fibroblasts

Ekaterina A. Savinova¹, Tatiana A. Salimova¹, Elena V. Proskurnina¹ , Ivan V. Rodionov¹, Olga A. Kraevaya², Pavel A. Troshin², Larisa V. Kameneva¹, Elena M. Malinovskaya^{1,*} , Olga A. Dolgikh¹ , Natalia N. Veiko¹ and Svetlana V. Kostyuk¹

¹ Research Centre for Medical Genetics, ul. Moskvorechye 1, 115522 Moscow, Russia

² Federal Research Center for Problems of Chemical Physics and Medicinal Chemistry of RAS, Semenov Prospect 1, 142432 Chernogolovka, Russia

* Correspondence: tigerilina@mail.ru

Abstract: The development of novel biologically active nanopharmaceuticals is a topical problem of medicine. Water-soluble fullerene derivatives are of particular interest due to their ability to regulate intracellular metabolism of reactive oxygen species (ROS) by direct oxidation or effects on oxidative and signaling enzymes. Here, we studied the effect of a water-soluble chlorine-containing derivative of C₆₀ fullerene on human embryonic lung fibroblasts. MTT tests, intracellular ROS visualization, detection of the ROS-associated gene and protein expression, repair, cell proliferation and cell cycle regulation, and quantitation of oxidative DNA damage were used. Within the first three hours after exposure, antioxidant effects were revealed. Later, oxidative damage appeared. Thus, the studied compound had an ambiguous effect on ROS metabolism associated with a switch in the regulatory effect, which must be taken into account when assessing its biological activity and toxicity.

Keywords: nanoparticles; fullerenes; reactive oxygen species; oxidative stress



Citation: Savinova, E.A.; Salimova, T.A.; Proskurnina, E.V.; Rodionov, I.V.; Kraevaya, O.A.; Troshin, P.A.; Kameneva, L.V.; Malinovskaya, E.M.; Dolgikh, O.A.; Veiko, N.N.; et al.

Effect of Water-Soluble Chlorine-Containing

Buckminsterfullerene Derivative on the Metabolism of Reactive Oxygen Species in Human Embryonic Lung Fibroblasts. *Oxygen* **2023**, *3*, 1–19.

<https://doi.org/10.3390/oxygen3010001>

Academic Editor: John T. Hancock

Received: 6 November 2022

Revised: 22 December 2022

Accepted: 23 December 2022

Published: 27 December 2022



Copyright: © 2022 by the authors. Licensee MDPI, Basel, Switzerland. This article is an open access article distributed under the terms and conditions of the Creative Commons Attribution (CC BY) license (<https://creativecommons.org/licenses/by/4.0/>).

1. Introduction

The progress in nanotechnology has allowed medicine to move far ahead in pharmacology. Among the most promising compounds considered as perspective nanodrugs are fullerenes and their derivatives [1]. Due to electronic structures and unique physical and chemical properties, fullerenes act both as pro-oxidants and as antioxidants [2,3]. This ability to either suppress or generate cytotoxic free radicals, together with a small size and a large surface area, leads to various applications in medicine [4,5]. The reactivity of fullerenes allows targeted surface modification and synthesis of water-soluble compounds with specified biological activity [6,7].

Chlorofullerene C₆₀Cl₆ can be used as a precursor for the synthesis of fullerene derivatives with high solubility in water and pronounced antibacterial and antiviral activity, including against human immunodeficiency virus [8–10]. Fullerene derivatives with five organic functional groups and chlorine atom attached to the cage can be synthesized as described elsewhere [10]. In general, organochlorine molecules are toxic (primarily hepatotoxic and nephrotoxic), examples of which are numerous, ranging from chloromethanes to dioxins [11] and chlorine-containing insecticides [12]. The inclusion of chlorine atoms in the molecules aggravates the toxicity [13]. The higher number of chlorine atoms causes a higher toxicity [14,15]. The mechanism of toxicity of halogen-containing organic substances lies in the induction of oxidative stress through various pathways [16,17].

Oxidative stress is a pathological state, where the production of reactive oxygen species prevails over the antioxidant defense, leading to disruption of signaling pathways, cellular

damage, and inflammation [18,19]. The family of reactive oxygen species is extremely diverse and heterogeneous; it includes low-molecular-weight organic compounds, transition metal ions, enzymes, and lipids. The network of antioxidants is also heterogeneous and numerous. Their effects depend on localization, the presence of co-antioxidants, and many other factors [20]. ROS metabolism are characterized by pleiotropy and double-edged effects. At low concentrations, ROS have physiological effects, participating in signal transduction, the cell cycle, and immune defense. It is the amount of ROS that determines the switching point from physiological to pathological effects. However, the shape of the “dose-effect” function is unique and unpredictable in each case [21]. Simultaneous participation of reactive oxygen species in several pathways makes it very difficult to interpretate their role in carcinogenesis [22]. Close relationships of oxidative stress, inflammation, and other types of metabolic stress necessitate a separate study of oxidative metabolism for different conditions and pathologies [23,24]. Understanding these mechanisms is important for development of new therapeutic strategies for diseases associated with the dysregulation of redox and oxidative metabolism.

The aim of the study was to investigate the effects of the C₆₀ derivative with one chlorine atom attached to the fullerene cage on ROS metabolism in human embryonic lung fibroblasts (HELFL) and to examine their safety and toxicity for further application.

2. Materials and Methods

2.1. Fullerene Derivative

Water-soluble buckminsterfullerene derivative **F1** (M = 1982.5) contains five residues of potassium salt of 3-phenylglutaric acid and one chlorine atom attached directly to the fullerene cage (Figure 1). Compound **F1** was synthesized in three steps from fullerene C₆₀. The details of the synthesis and the spectral data for compound **F1** were published previously [25]. The scheme of the synthesis is also given in Figure S1.

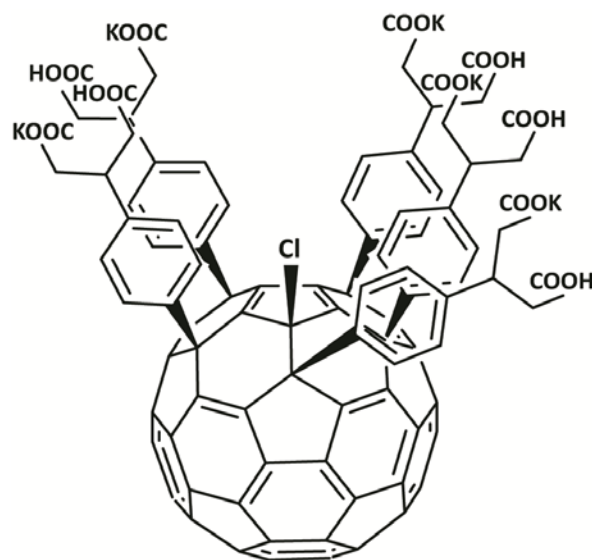


Figure 1. The molecular formula of **F1**.

To reveal aggregation of the fullerene derivative in an aqueous solution, we performed dynamic light scattering measurements using a Photocor Complex spectrometer at 23 °C with a near infrared laser (790 nm). The fullerene derivative **F1** (4 mg) was dissolved in 4 mL of deionized water. The solutions were filtered through a polyethersulfone syringe filter (0.45 µm) to 4 mL glass vial. The results are given in Figure S2. As most of the amphiphilic fullerene derivatives, water-soluble compound **F1** forms bilayer vesicles with an average hydrodynamic radius (R_h) of ~50 nm in aqueous solutions.

The fluorescence and absorption spectra are presented in Figures S3 and S4, respectively.

2.2. Cell Culture

Human embryonic lung fibroblasts (HELFL) (4th passaging cells) were supplied by the Research Centre for Medical Genetics. Cultivation was performed at 37 °C using a DMEM medium (PanEco Moscow, Russia), 10% fetal calf serum (PAA, Vienna, Austria), penicillin (50 U/mL), streptomycin (50 µg/mL), and gentamicin (10 mg/mL). The cells were cultured for 2 or 24 h, as described previously [26,27]. The cells were incubated with the fullerene for 1 h, 3 h, 24 h, and 72 h.

2.3. MTT Test

The MTT (3-(4,5-dimethylthiazol-2-yl)-2,5-diphenyltetrazolium bromide) tetrazolium reduction assay was used to assess cell viability. The details are described in [26,27]. The cells were prepared in 96-well plates and incubated for 72 h. Fluorescence was measured at 550 nm with an EnSpire Plate Reader (EnSpire Equipment, Turku, Finland). As a negative control, the cells were incubated with a culture medium and deionized water (a solvent for the fullerene). As a positive control, the fullerene F1 was used in a high concentration (600 µM).

2.4. Antibodies

DyLight488-γH2AX (pSer139) primary antibodies (nb100-78356G; NovusBio, Centennial, CO, USA), FITC-NRF2, (bs1074r-fitc; Bioss Antibodies Inc., Woburn, MA, USA), FITC-BRCA1 (Nb100-598F; NovusBio, Centennial, CO, USA), PE- 8-oxo-dG (sc-393871 PE; Santa Cruz Biotechnology, Dallas, TX, USA), CY5.5-NOX4 (bs-1091r-cy5-5; Bioss Antibodies Inc., Woburn, MA, USA), A350-BCL2 (bs-15533r- a350; Bioss Antibodies Inc., Woburn, MA, USA), BAX (Nb120-7977; NovusBio, Centennial, CO, USA), and secondary anti-rabbit IgG-FITC (sc-2359; Santa Cruz Biotechnology, Dallas, TX, USA) were used.

2.5. Flow Cytometry

The cells were treated with Versene solutions (Thermo Fisher Scientific, Waltham, MA, USA) and 0.25% trypsin (Paneco, Moscow, Russia). Next, the cells were washed with culture medium and suspended in phosphate buffer solution (pH 7.4) (Paneco, Moscow, Russia). Paraformaldehyde (Sigma-Aldrich, St. Louis, MO, USA) was used for cell fixation (37 °C for 10 min). Next, the cells were washed thrice with a BSA–PBS mixture (0.5%). After treatment with 0.1% Triton X-100 solution in PBS for 15 min at 20 °C, the cells were washed thrice with 0.5% BSA–PBS solutions. For staining, the cells were treated with conjugated antibodies (1 µg/mL) for 2 h at 20 °C and washed with phosphate-buffered saline. As for reaction with unconjugated primary antibodies to BAX, the cells were incubated with the antibodies (1 µg/mL) for 8 h (+4 °C), washed with 0.5% BSA–PBS solutions, incubated for 1 h at 20 °C with secondary antibodies (1 µg/mL) and washed thrice with 0.5% BSA–PBS solutions.

A flow cytometer (CytoFlex S; Beckman Coulter, Pasadena, CA, USA) was used for the measurements.

To assess intracellular ROS, the suspension of the cells was incubated for 15 min in the dark with H2DCFH-DA solutions in phosphate-buffered saline (10 µM; Molecular Probes/Invitrogen, Carlsbad, CA, USA), washed and resuspended in PBS. The measurements were performed using the FITC channel of the flow cytometer.

2.6. Fluorescence Microscopy

Fluorescence imaging of the cells was performed with an Axio Scope.A1 microscope (Carl Zeiss, Jena, Germany). After fixing with 3.7% formaldehyde (20 min, +4 °C), the cells were treated with 0.1% Triton X-100 in PBS and washed and treated with 1% albumin solution in PBS. Next, the cells were incubated overnight at +4 °C with primary antibodies FITC-NRF2 (bs1074r-fitc) and CY5.5-NOX4 (bs-1091r-cy5-5) (1 µg/mL in PBS + 1% BSA) (Bioss Antibodies Inc., Woburn, MA, USA). Next, the cells were washed with PBS and stained with DAPI.

2.7. Spectrophotometry and Spectrofluorimetry

A CLARIOstar reader (BMG Labtech, Ortenberg, Germany) was used to register fluorescence and absorption spectra of **F1** in aqueous solutions and culture media (Figure S3).

2.8. Immunocytochemistry

Cells on 25 cm³ slides (Thermo Fisher Scientific, Waltham, MA, USA) were fixed in paraformaldehyde (3%) at 4 °C for 20 min, then washed with phosphate-buffered saline and permeabilized with Triton X-100 (0.1%) in phosphate-buffered saline for 15 min (20 °C). Next, the cells were treated with BSA–PBS solutions (0.5%) for 1 h and incubated at 4 °C with antibodies for 8 h. The cells were washed with Triton X-100 (0.1% in PBS), incubated for 2 h (20 °C) with FITC goat anti-mouse IgG, washed with phosphate-buffered saline and stained with DAPI (4', 6-diamidino-2-phenylindole) [26,27].

2.9. Intracellular ROS Assay

ROS detection was performed using three methods: flow cytometry, fluorescence microscopy, and total fluorescence analysis in a 96-well plate. Cells in 96-well plates were incubated with **F1**, washed with phosphate-buffered saline and treated with H2DCFH-DA (10 µM in PBS) (Molecular Probes/Invitrogen, Carlsbad, CA, USA), and the total fluorescence was analyzed at $\lambda_{ex} = 503$ nm and $\lambda_{em} = 524$ nm (EnSpire Equipment, Turku, Finland) at 37 °C 10 times at 5 min intervals. The reaction rate constant of DCF formation (k) was calculated using the function of DCF fluorescence vs. the incubation time with H2DCFH-DA. The ratio k_i/k_0 was calculated, where k_i and k_0 are the rate constants of ROS formation in the presence of fullerene and in the control, respectively. The average value of DCF fluorescence for 16 wells and standard deviation were calculated and presented below.

2.10. mRNA Quantification

A RNeasy Mini Kit (Qiagen, Hilden, Germany) was used for isolation of total mRNA. After treatment with DNAase I, a reverse transcriptase kit (Silex, Moscow, Russia) was used to perform reverse transcription. qRT-PCR with SYBR Green PCR Master Mix (Applied Biosystems, Foster City, CA, USA) was applied for obtaining the expression profiles. The measurements were performed with StepOnePlus (Applied Biosystems). The primers were as follows (Syntol, Moscow, Russia): *BRCA1* (F: TGTGAGGCACCTGTGGTGA, R: CAGCTCCTGGACTGGTAGAG); *NRF2* (NFE2L2) (F: TCCAGTCAGAAACCAGTGGAT, R: GAATGTCTGCGCCAAA AGCTG); *NOX4* (F: TTGGGGCTAGGATTGTGCTA, R: GAGTGTTCGGCA-CATGGGTA); *BRCA2* (F: CCTCTGCCCTTATCATCACTTT, R: CCAGATGATGTCTT CTC-CATCC); *CCND1* (F: TTCGTGGCCTCTAAGATGAAGG, R: GAGCAGCTCCATTTGCAGC); *CDKN1A* (F: TGTCCGTCAGAACCCATGC, R: AAAGTCGAAGTCCATCGCTC); *0* (F: ATG-GAGCCTTCGGCTGACT, R: GTA ACTATTTCGGTTCGGTGGG); and *TBP* (a reference gene) (F: GCCCGAAACGCCGAATAT, R: CCGTGGTTCGTGGCTCTCT).

2.11. Gene Accession Numbers

NADPH oxidase 4 [Homo sapiens (human)] (*NOX4*) Gene ID: 50507; NFE2 like bZIP transcription factor 2 [Homo sapiens (human)] (*NFE2L2*) Gene ID: 4780; BRCA1 DNA repair associated [Homo sapiens (human)] (*BRCA1*) Gene ID: 672; CCND1 cyclin D1 [Homo sapiens (human)] (*CCND1*) Gene ID: 595; CDKN1A cyclin dependent kinase inhibitor 1A [Homo sapiens (human)] (*CDKN1A*) Gene ID: 1026; CDKN2A cyclin dependent kinase inhibitor 2A [Homo sapiens (human)] (*CDKN2A*) Gene ID: 1029; TBP TATA-box binding protein [Homo sapiens (human)] (*TBP*) Gene ID: 6908.

2.12. Statistics

The experiments were performed in triplicates. The data are given as the mean and standard deviation (SD). The statistical significance was calculated with the nonparametric Mann–Whitney test; the significant differences ($p < 0.01$) are marked with “*” in the charts. StatPlus2007 software (AnalystSoft Inc., Walnut, CA, USA) was used for data analysis.

3. Results

3.1. Cytotoxicity and Cell Penetration

The cytotoxic effect of **F1** was assessed with a conventional MTT test. The effect of **F1** on HELF was studied in the concentration range from 0.009 μM to 600 μM . The fullerene was added to the medium, and the cells were cultured for 1–24 h. **F1** was not toxic at concentrations below 14 μM . At concentrations from 14 μM to 171 μM , **F1** caused less than 50% cell death. At concentrations above 171 μM , this compound showed pronounced toxicity (Figure 2). The positive control was performed with dimethyl sulfoxide (0.0001–50%) (Figure S5).

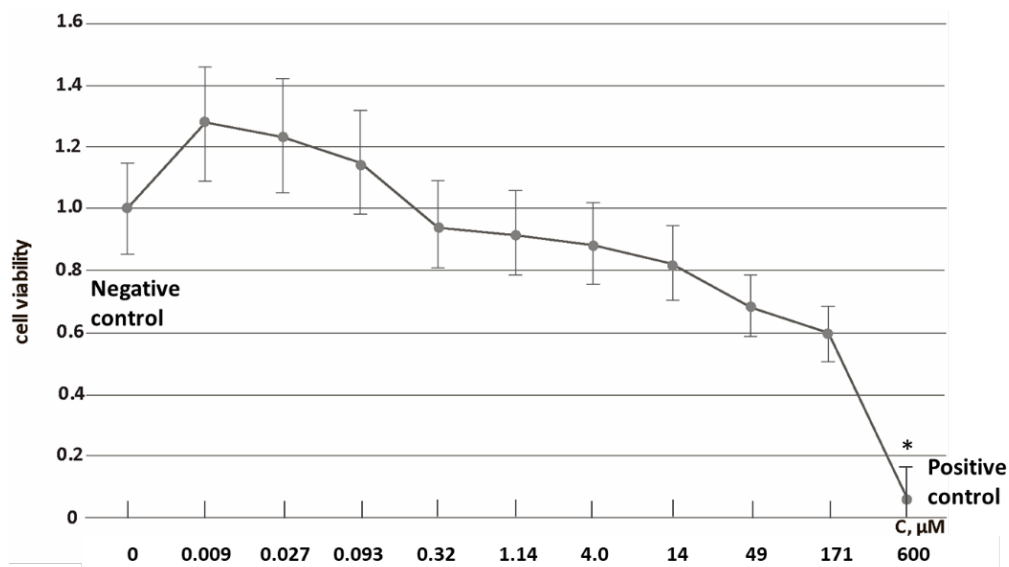


Figure 2. MTT-test result: the absorbance at 570 nm vs. **F1** concentration. Significant differences with the negative control by the Mann–Whitney test ($p < 0.01$) are denoted by “*”.

The concentrations of 0.009 μM that is the lowest concentration effecting the cell survival and 14.0 μM that is the maximum non-toxic concentration of **F1** causing damage to no more than 20% of cells restrict the interval of non-toxic and biologically active concentrations. Thus, these concentrations were used for the study.

Fluorescence excitation spectra ($\lambda_{\text{ex}} = 230\text{--}600$ nm, $\lambda_{\text{fl}} = 620$ nm) for the solution of **F1** in the culture medium demonstrated two excitation maxima at 280 nm and 370 nm (Figure S3a). There are three emission maxima at 436, 470, and 628 nm (Figure S3b) and one maximum $\lambda_{\text{fl}} = 628$ nm at $\lambda_{\text{ex}} = 370$ nm (Figure S3c).

Based on these data, we studied the penetration and the localization of **F1** in cells using the red region of the spectrum. Within 1–24 h of incubation, **F1** penetrates through the cell membrane and accumulates in the cytoplasm (Figure 3a). Flow cytometry of unfixed HELFs ($\lambda_{\text{ex}} = 488$ nm) confirmed the results of fluorescence microscopy. The fluorescence in cells increased with the increasing cultivation time (Figure 3b).

Thus, the fluorescence of **F1** makes it possible to study its penetration into cells, accumulation, and localization in the cytoplasm.

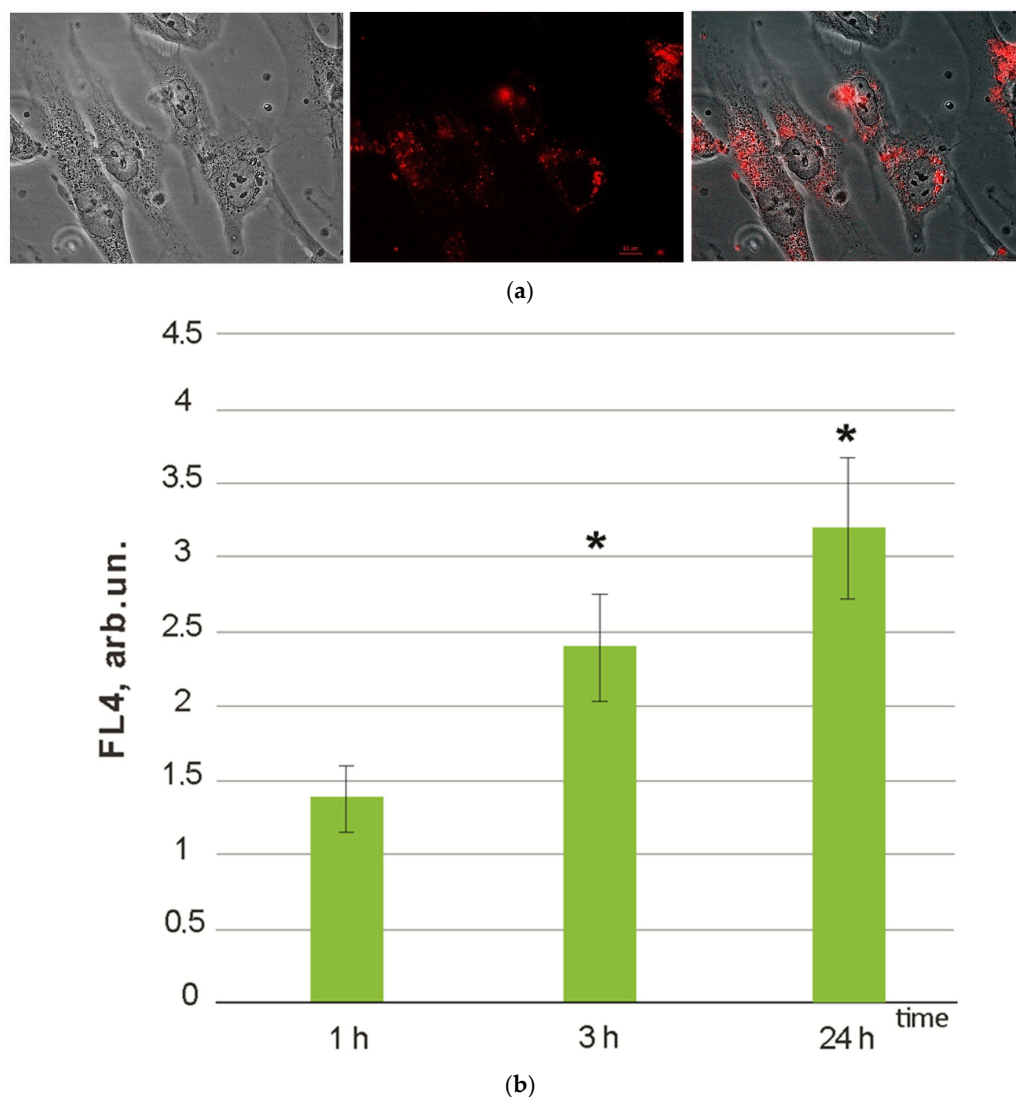


Figure 3. (a) Fluorescence images of HELFs (40 \times) incubated with F1 (1.5 μ M) for 3 h in transmitted light (left), fluorescence (middle), and merged mode (right) using a 575–645 nm excitation filter (#6) and a 530–555 nm emission filter; (b) median values of FL4 signal in non-fixed cells vs. cultivation time. “*” - According to the Mann–Whitney test, the signals after 3 and 24 h differed significantly from the control value ($p < 0.01$).

3.2. Intracellular ROS and NOX4 Gene Expression

The compound H2DCFH-DA (2,7-dichlorodihydrofluorescein diacetate), which is a dye that rapidly penetrates through cell membranes and is hydrolyzed fast to DCFH in the cytosol by cell hydrolases, was used to assess intracellular ROS. Non-fluorescent DCFH reacted to intracellular oxidative stress, being oxidized to intensely fluorescent DCF (dichlorofluorescein) by ROS.

Figure 4 shows the rate constants of DCF synthesis in the cells at F1 concentrations of 0.009 μ M and 14.0 μ M vs. the control (cells cultured without fullerene) on time (1, 3, 24, and 72 h of incubation of cells with the compound). Adding 14.0 μ M F1 to the cells resulted in a statistically significant decrease (by $\approx 40\%$) of ROS after 1 and 3 h. Adding 0.009 μ M resulted in a tendency to decrease ROS by 12% and 18% after 1 and 3 h, respectively.

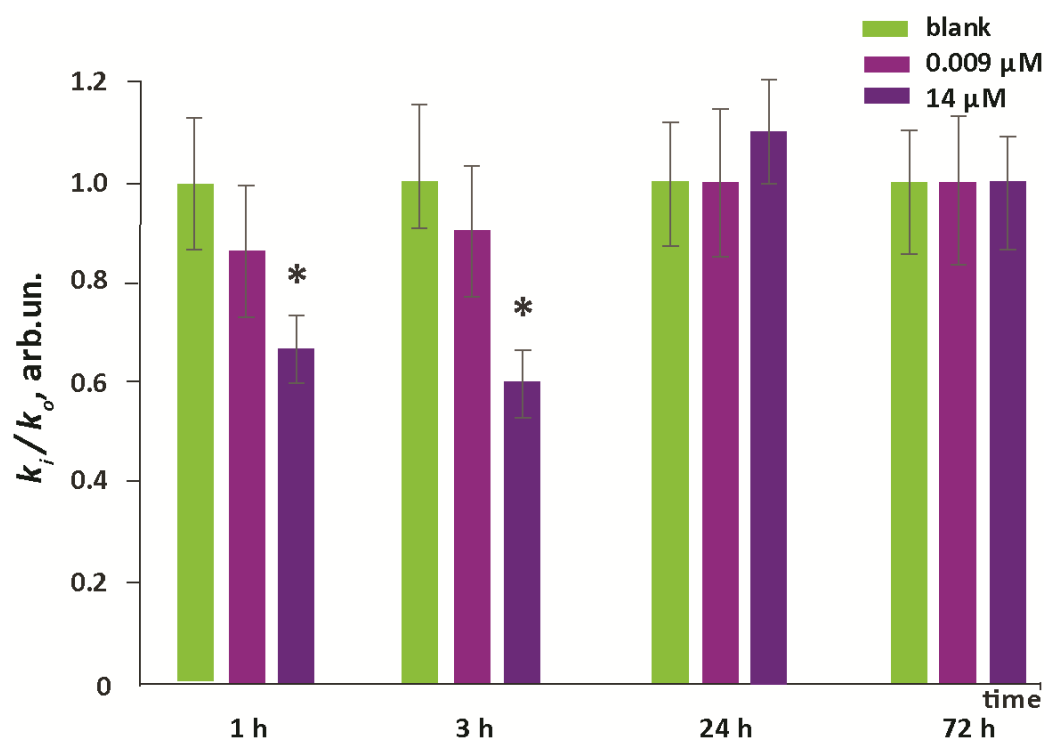
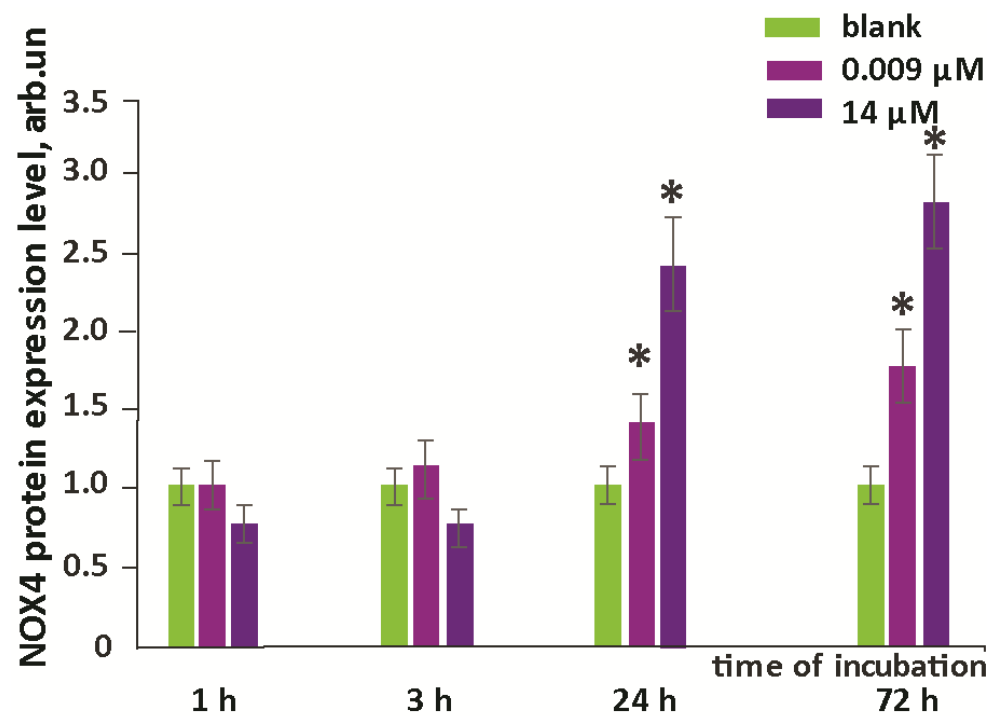


Figure 4. Histograms of ROS levels in cells (the ratio of DCF synthesis rate constants k_i to the control value k_o) at various F1 concentrations and incubation times (indicated in the figure). Significant differences with the control by the Mann–Whitney test ($p < 0.01$) are denoted by “*”.

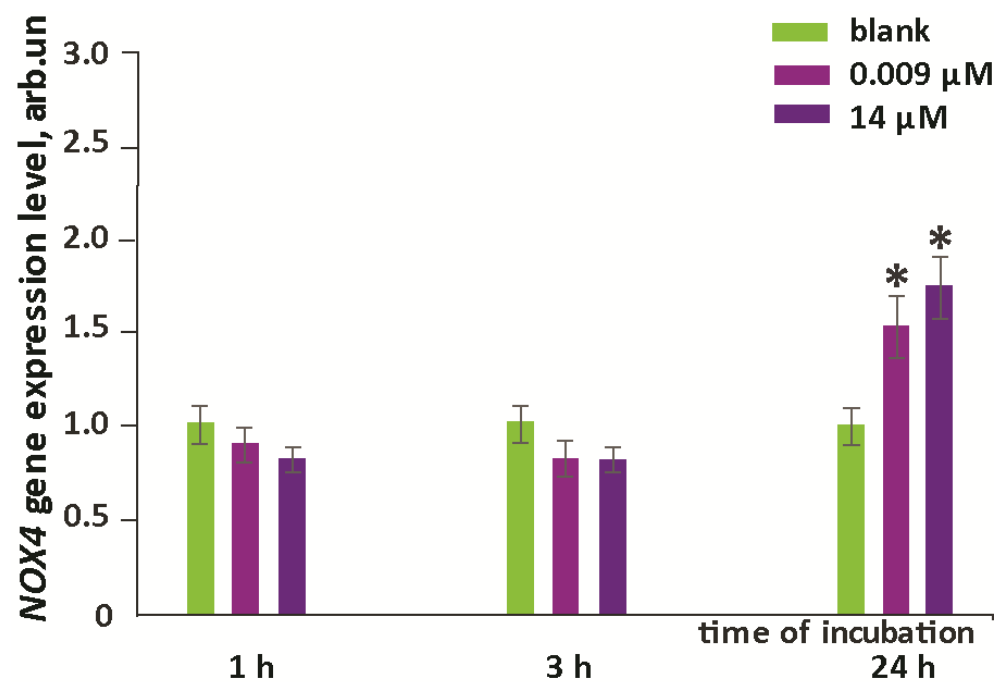
Thus, during the first three hours after incubation, F1 contributed to a decrease in the intracellular ROS, but within a day this effect disappeared. Probably, because of biochemical transformation, this compound lost its antioxidant properties, or it led to increased expression of ROS by enzymes, in particular NADPH-oxidase, which is the main source of physiological low-level intracellular ROS. NOX4 was expressed in fibroblasts, and its expression was regulated at the gene level.

When the cells were exposed to F1 (0.009 μM and 14.0 μM), the NOX4 expression increased by a factor of 1.5–2.8 at the gene and protein levels 24–72 h after the start of incubation (Figure 5).

The increase in NOX4 protein expression after 24 h may explain the increase in intracellular ROS after 24–72 h and the possible development of ‘prolonged’ oxidative stress (see below).



(a)



(b)

Figure 5. NOX4 protein (a) and NOX4 gene expression (b) relative to the control values in HELF cells after the incubation with F1. *TBP* was used as an internal standard gene. Significant differences with the control by the Mann–Whitney test ($p < 0.01$) are denoted by “*”.

3.3. NRF2 Expression

The transcription factor NRF2 participated in the regulation of the antioxidant response of cells. The *NRF2* gene expression increased by 8 and 10 times in 1 and 3 h, respectively,

after adding F1 at a concentration of 14.0 μM to HELFs, while adding 0.009 μM had no effect on NRF2 gene expression (Figure 6a).

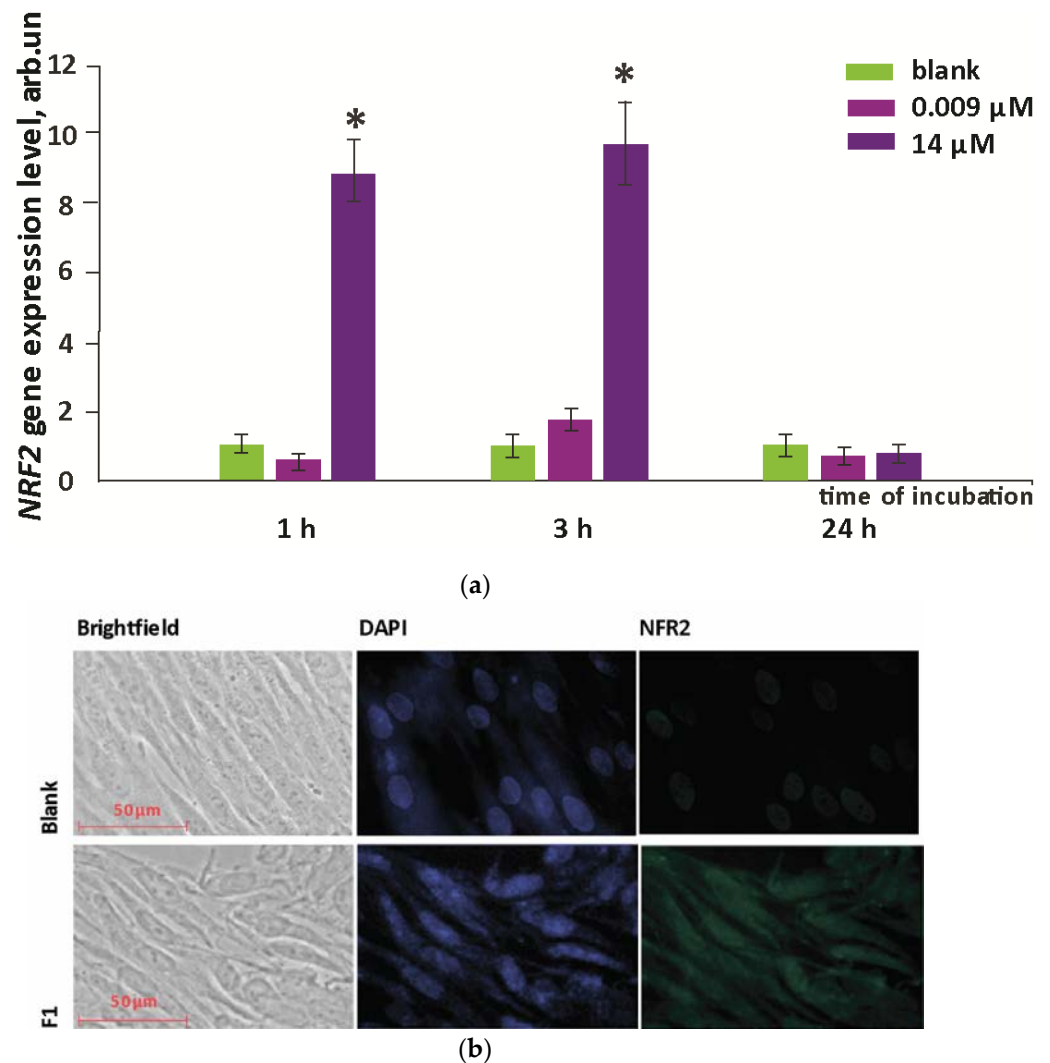


Figure 6. The NRF2 gene expression (a) in HELF cells incubated with F1. The NRF2 RNA amount is a mean value from three experiments of NRF2 gene expression in the presence of F1 relative to the control value. TBP was used as an internal standard gene. Significant differences with the control by the Mann–Whitney test ($p < 0.01$) are denoted by “*”. (b) Microscopy images at a magnification of 40 \times : (top to bottom) the control culture, cells after incubation with F1 (14.0 μM) for 24 h; (left to right) visible light, DAPI staining of nuclei (340–370 nm excitation filter, 420–470 emission nm), and fluorescence of antibodies to NRF2 (450–490 nm excitation filter (#4), 500–550 nm emission).

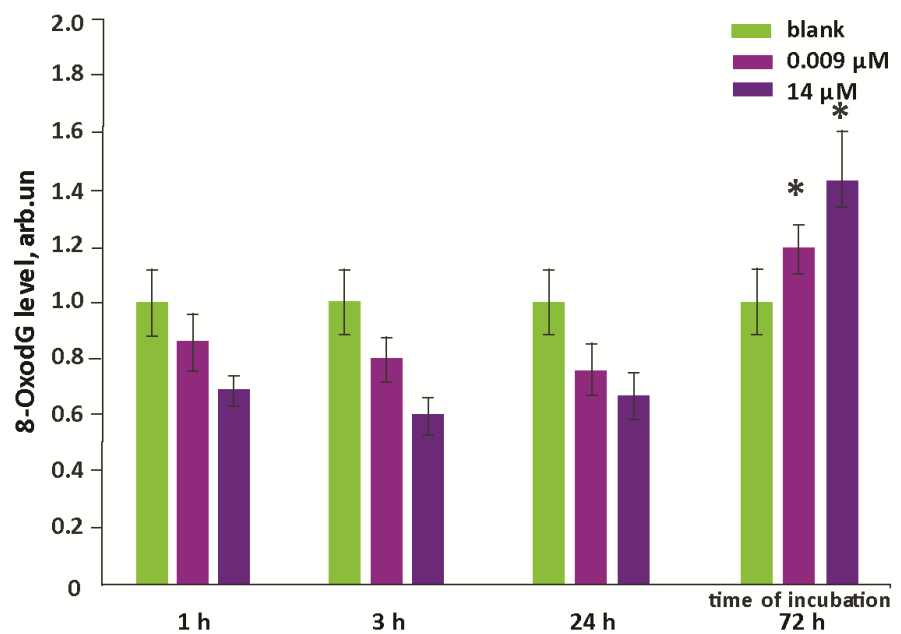
Flow cytometry data were confirmed by fluorescence images. After 3 h, the NRF2 protein level increased by approximately 2-fold when F1 (14.0 μM) was added and by 1.5-fold after 24 h, with NRF2 localized in both nucleus and cytoplasm of the cells (Figure 6b).

The increased NRF2 gene expression during the first hour apparently explained the effective decrease in intracellular ROS within 1–3 h.

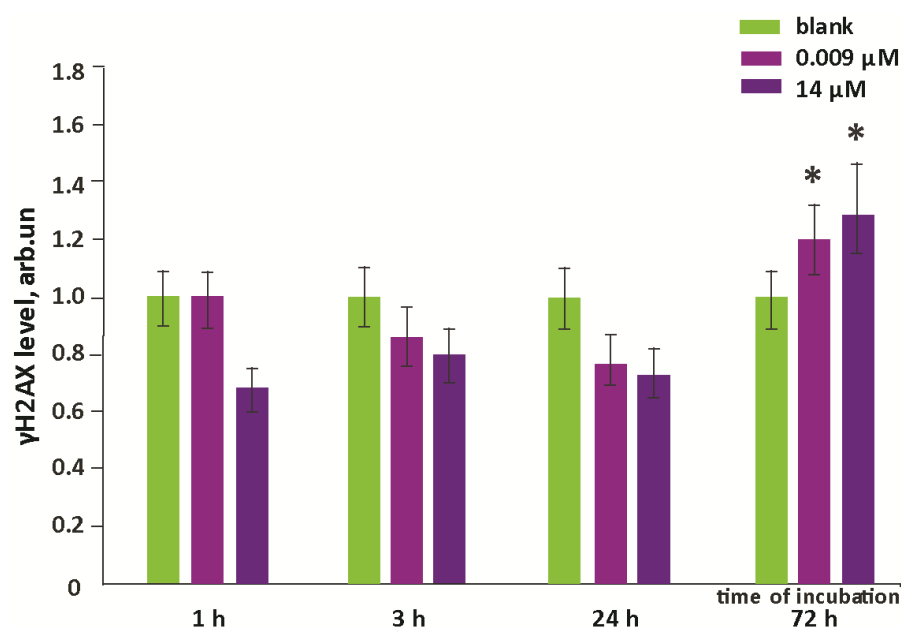
3.4. Oxidative Damage to DNA and Activation of Repair Genes

The possible damaging effect on the cell as a result of increased ROS synthesis can be realized through DNA oxidative modifications and breaks.

In the presence of F1 (0.009 μM and 14.0 μM), the DNA oxidative modifications increased by 20–40% in 72 h compared to the control (Figure 7a), which is most likely a consequence of the increase in intracellular ROS after 24 h in the presence of the fullerene.



(a)



(b)

Figure 7. Histograms of DNA oxidation marker 8-oxyguanosine (a) and phosphorylated histone form in H2AX (b) in HELFs after incubation with F1 (medians are given). Significant differences with the control by the Mann–Whitney test ($p < 0.01$) are denoted by “*”.

Increased levels of 8oxodG can lead to DNA breaks. Detection of DNA double-strand breaks is based on the phosphorylation of serine residue 139 at the DNA break site involving ATM kinase, ATR, and DNA-PK by a conserved histone protein involved in DNA chromatin packaging (H2AX). Bound to the labeled antibodies, phosphorylated histones γH2AX were visualized in the cell nucleus; their enhanced accumulation proved increased levels of

nuclear DNA double-strand breaks. Using flow cytometry (comparing the medians), we revealed that incubation with F1 (0.009 μM and 14.0 μM) within 72 h resulted in an increase in DNA double-strand breaks by 20–30% (Figure 7b) that correlated with raised oxidative modifications of nuclear DNA.

As a result of DNA damage, the genes involved in DNA repair were activated, with one of such genes being the BRCA1 gene. When cells were exposed to the incubation with F1 (0.009 μM and 14.0 μM), the levels of BRCA1 gene and protein expression did not change for 72 h (Figure 8).

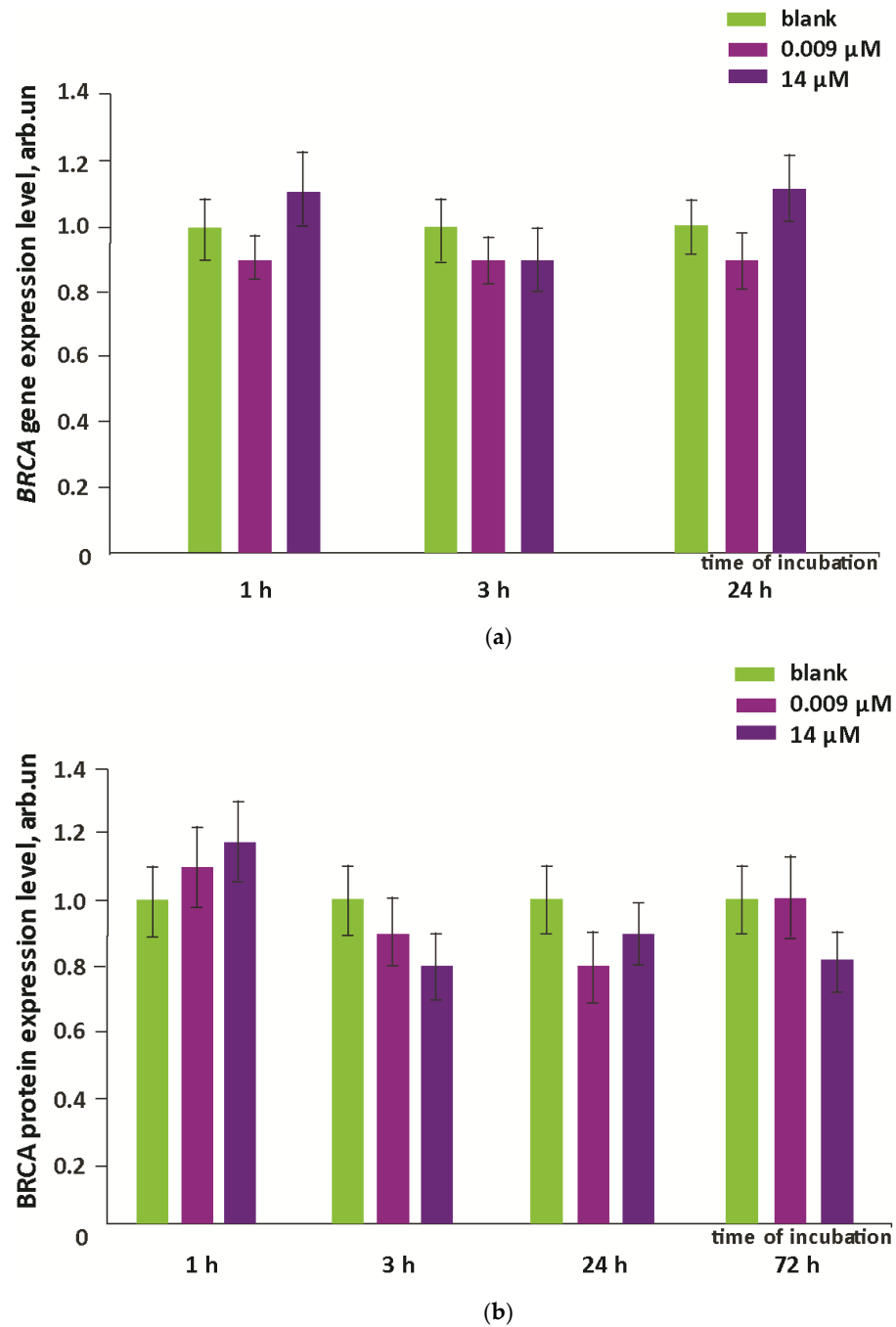


Figure 8. Expression of *BRCA1* gene (a) and BRCA1 protein (b) in HELF cells after incubation with F1. The amount of *BRCA1* RNA is the average of three measurements related to the control values. *TBP* was used as an internal standard gene. Significant differences with the control by the Mann–Whitney test ($p < 0.01$) are denoted by “**”.

3.5. Proliferation and Apoptosis

DNA breaks can be repaired with cell cycle arrest. Moreover, cells can activate a programmed cell death program (apoptosis). Using the MTT test, we found the increased proliferative activity of HELFs after 72 h in the presence of **F1** (0.009 μM); the number of cells in the population increased by $\approx 20\%$.

At the beginning of the cell cycle, cyclin D1 protein encoded by the *CCND1* gene starts to be synthesized. Cyclin D1 triggers the G1 phase regulating cell transition to the S phase. Cyclin-dependent kinase inhibitors belong to cell cycle regulators. The kinase inhibitor p21 negatively influences the activity of cyclin-dependent kinase (CDK) complexes in the G1 phase of the cell cycle; increased expression of the p21 gene (*CDKN1A* gene) can result in G1 arrest. The *CDKN2* gene encodes the p16 protein, a cell cycle regulator that, by binding to CDK4 and CDK6, disrupts cyclin D1 binding to CDK. The complicated system regulation of cell cycle genes leads to either progression or inhibition of the cell cycle.

Incubation with **F1** (0.009 μM) resulted in an increase in *CCND1* gene expression by 2–3 times and inhibition or no change in expression of *CDKN1A* and *CDKN2* genes (Figure 9a–c), which reflects an increase in cell cycle progression and explains a $\approx 20\%$ increase in the cell population after 3 days of incubation in the presence of **F1**. When cells were exposed to a concentration of 14.0 μM , a 2–6-fold increase in *CCND1* gene was observed for 1–3 h and inhibition of *CCND1* gene expression after 24 h. At the same time, the expression of *CDKN1A* and *CDKN2* genes in HELFs increased by 2–8-fold for 1–24 h (Figure 9a–c). The high level of kinase inhibitor expression leads to a decreased cell cycle progression and explains the $\approx 20\%$ decrease in the number of cells in the population after 3 days of cultivation of HELFs in the presence of **F1** (14.0 μM).

The enhancement of proliferative activity of HELFs in the presence of small amounts of **F1** was indicated by the level of proliferation marker Ki-67, which increased by a factor of 1.8–2.4 within 1–72 h after adding **F1** at the concentration of 0.009 μM (Figure 9d). For 14.0 μM , the Ki-67 level increased by a factor of 1.3–2.3 within 1–3 h and decreased after 24–72 h.

Changes in the number of cells in the population depended on both cell cycle progression and apoptosis. The effect of **F1** on the expression of proapoptotic (BAX) and anti-apoptotic (BCL2) proteins has been studied.

When cells were exposed to **F1** at the concentration of 0.009 μM for 1–72 h, an increase in the expression of anti-apoptotic protein BCL2 and inhibition of ≈ 2 -fold expression of proapoptotic protein BAX (Figure 10a), which indicates inhibition of apoptosis and increases the number of cells in the population, were observed. For 14.0 μM , the level of proapoptotic protein BAX was increased by 1.5–2 times, and the amount of anti-apoptotic protein BCL2 was inhibited or not changed for 1–72 h (Figure 10b). A high level of proapoptotic protein and a decrease in the expression level of anti-apoptotic protein increased cell apoptosis and decreased the number of cells in the population.

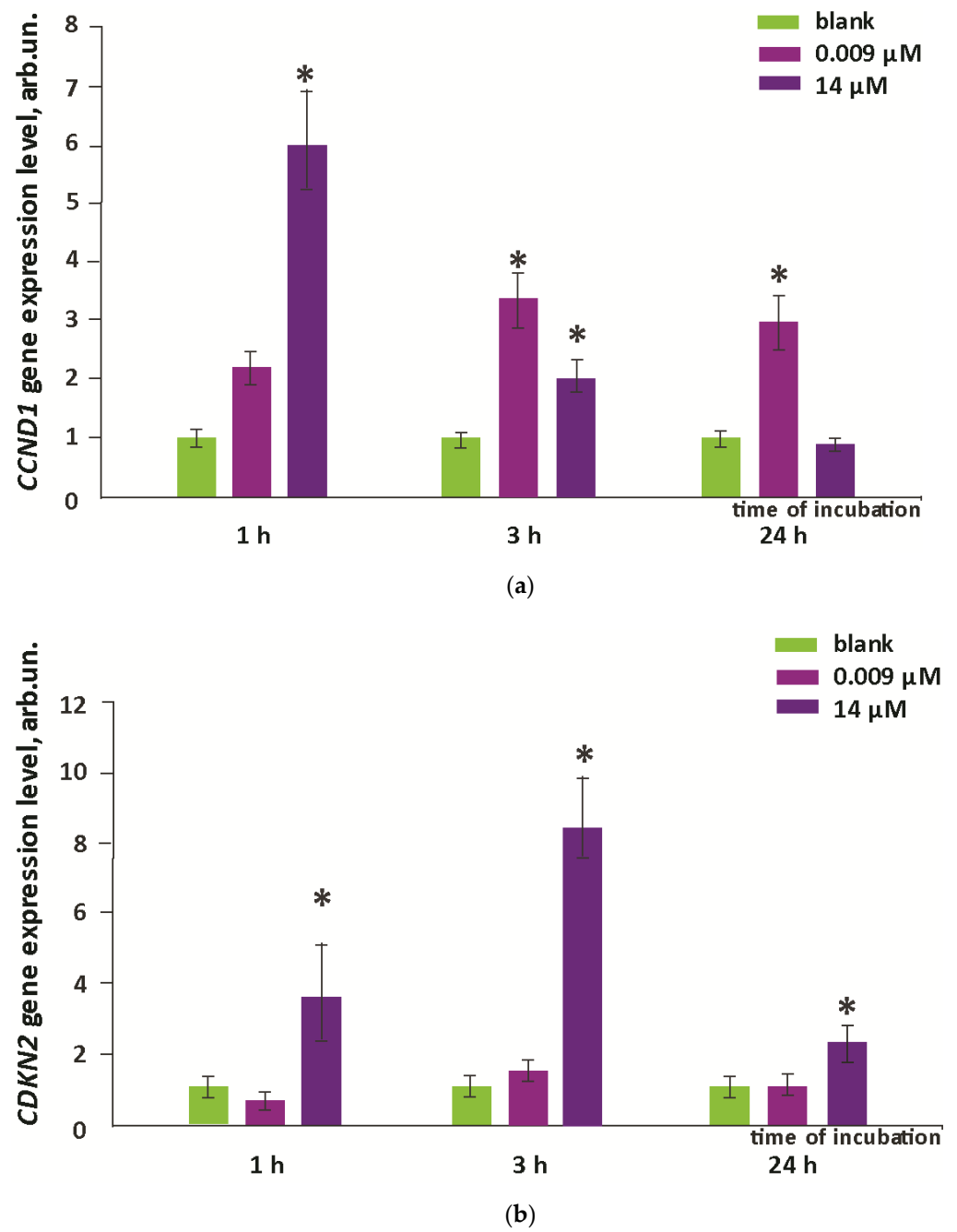
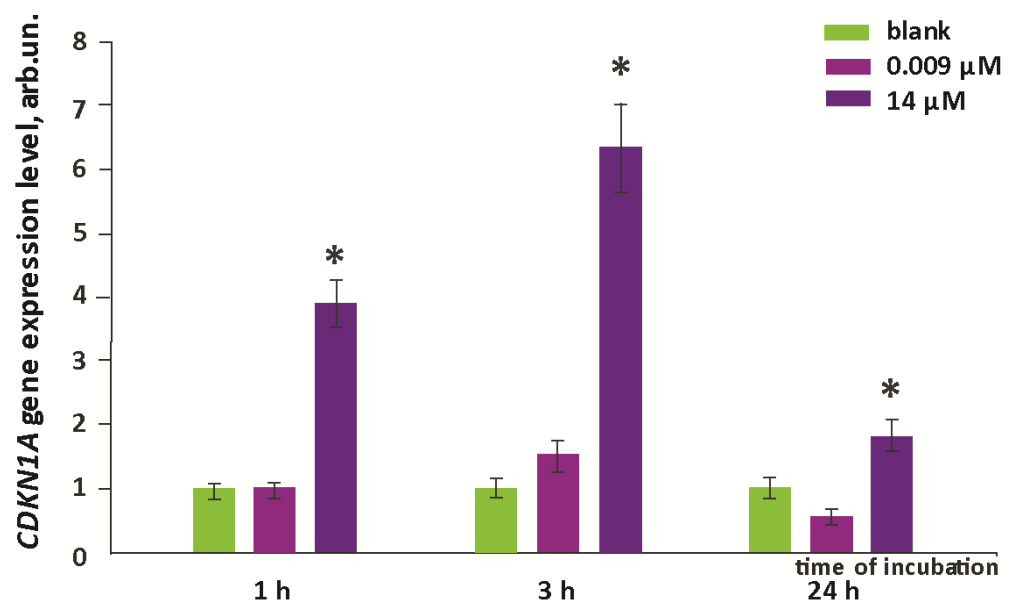
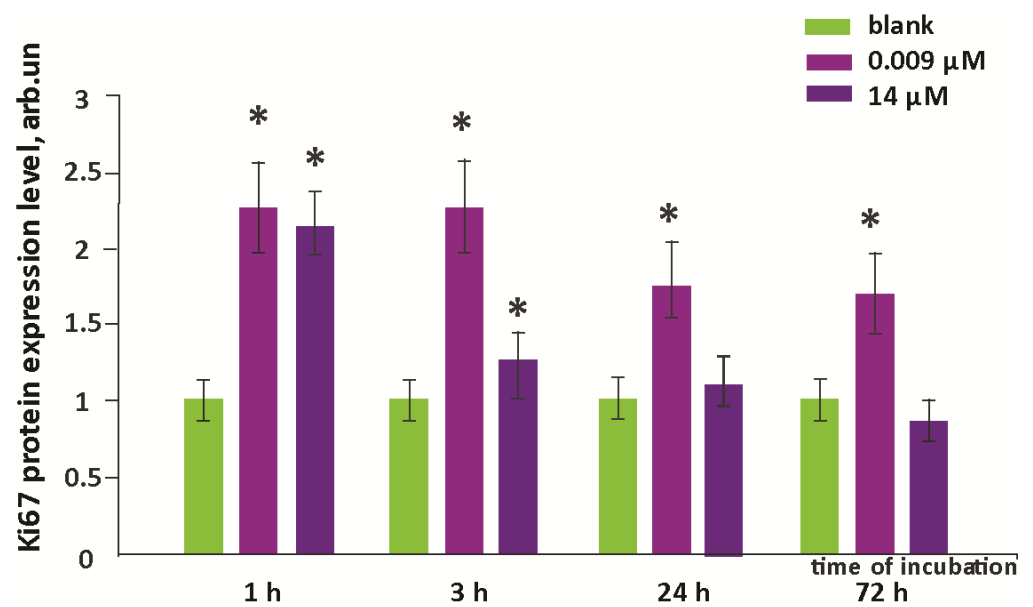


Figure 9. Cont.



(c)



(d)

Figure 9. Expression of *CCND1* (a), *CDKN2* (b), and *CDKN1A* (c) genes in HELF cells. The number of RNA genes is the average from three experiments related to the control value. *TBP* was used as an internal standard gene. The level of Ki-67 protein (d) in HELFs treated with F1 relative to control values (cells cultured without the fullerene) is shown. Significant differences with the control by the Mann–Whitney test ($p < 0.01$) are denoted by “*”.

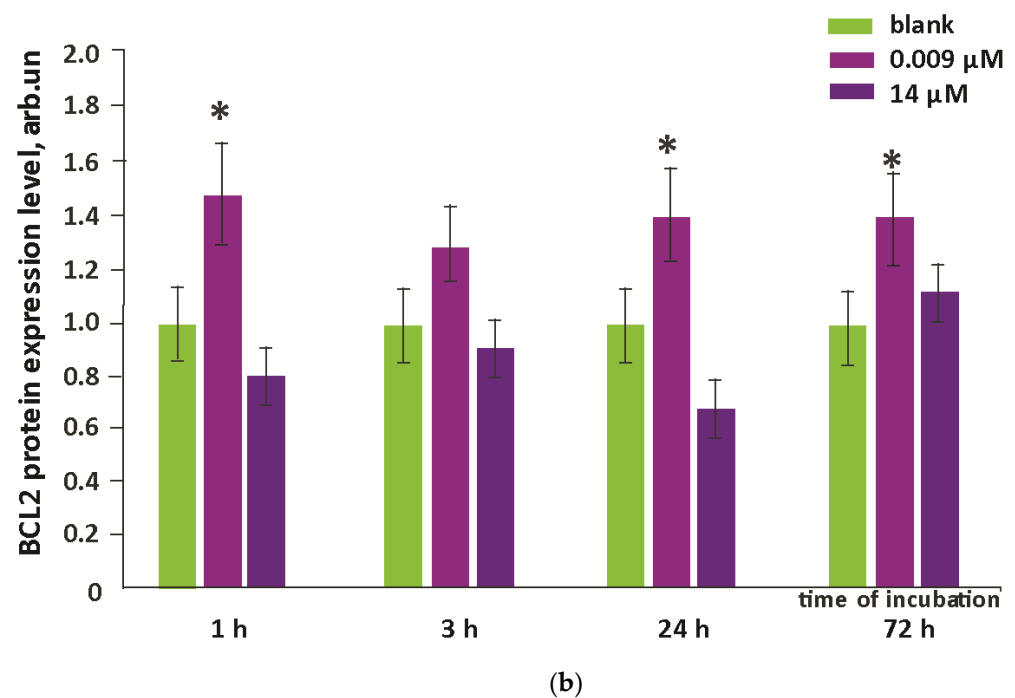
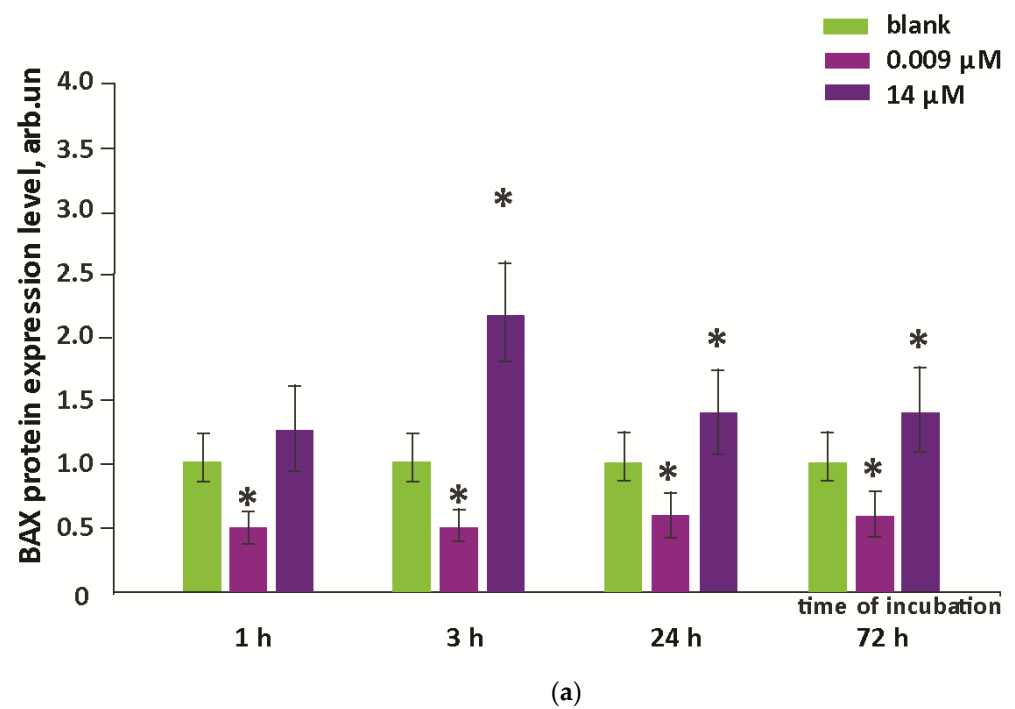


Figure 10. Expression of BAX (a) and BCL2 (b) proteins in HELF cells treated with F1 related to the control values (cells cultured without the fullerene). Significant differences with the control by the Mann-Whitney test ($p < 0.01$) are denoted by “*”.

4. Discussion

Let us summarize the main results of the study (Figure 11):

1. Within 1–24 h of incubation, F1 penetrated through the cell membrane and accumulates in the cytoplasm.
2. During the first three hours after incubation, the level of intracellular ROS dropped by about 40% (for the higher concentration). Then, within a day, it was restored to the initial level, and then it did not change.

3. During the first hour for the higher concentration of **F1**, the expression of the *NRF2* gene, which was responsible for the anti-inflammatory and antioxidant response of the cell, increased by an order of magnitude; this increase was not a compensatory response to oxidative stress; thus, the studied compound is probably an activator of the NRF2 pathway.
4. In contrast, NOX4 expression increased by about 2.5-fold after one day of incubation (for both concentrations studied) and remained at about the same level after three days.
5. Oxidative damage of DNA occurred on the third day after incubation, while the activity of repair genes did not change.

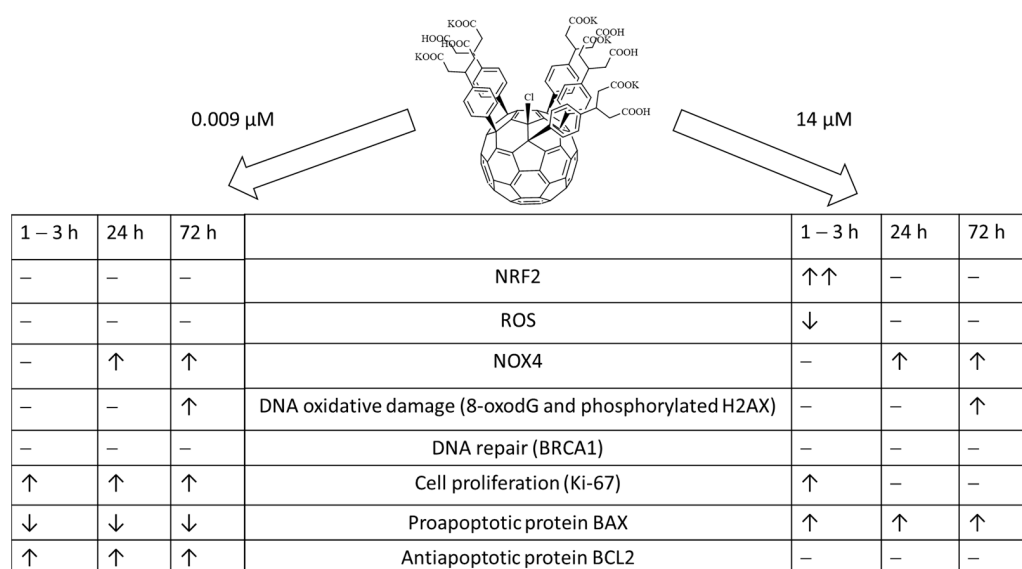


Figure 11. Effects of **F1** at the minimum effective and the maximum non-toxic concentrations on human embryonic lung fibroblasts.

The effect of **F1** on the cell cycle depended on the concentration. For a low concentration, we observed inhibition of apoptosis and increased proliferation throughout the time interval. For a high concentration, proliferation was observed in the first 1–3 h. Later, there was activation of apoptosis, resulting in a decrease in proliferative activity to the control level.

Two unidirectional effects are observed within the first 3 h, namely, the activation of the NRF2 pathway and the reduction of intracellular reactive oxygen species (primarily hydrogen peroxide). NRF2 transcription factor plays key role in regulation of the protecting expression of antioxidant proteins. In the absence of stress, NRF2 is retained in the cytoplasm by Kelch-like-ECH-associated protein 1 (KEAP1) and Cullin 3, which by ubiquitination degrades it [28]. Oxidative stress promotes the destruction of critical cysteine residues in KEAP1 molecules, thus disrupting NRF2 ubiquitination, which begins to accumulate in cells and is transported to the nucleus, where it forms a heterodimer with one of the musculoaponeurotic fibrosarcoma (MAF) protein and antioxidant response elements (ARE) included in the pro-rectal region of many antioxidant genes, which initiates their transcription [29]. Hypothetically, the fullerene derivative **F1** for the first 1–3 h prevents NRF2 binding to cytoplasmic proteins and then induces the expression of cytoprotective proteins genes, such as NAD(P)H-quinone oxidoreductase 1, the catalytic subunit of glutamate-cysteine ligase, the regulatory subunit of glutamate-cysteine ligase, and hemoxygenase-1. NRF2 activation may explain the increased proliferation in the first three hours after incubation.

Thus, in the first three hours, the scale of ROS metabolism was shifted to the “antioxidant side” (for a higher concentration), which can even be considered as “antioxidative” or

“reductive stress” in the presence of damage or pathological processes in the cell [30,31]. No significant changes were found for the lower concentration compared to the control, but Figure 4 demonstrates a downward trend in intracellular ROS (mainly hydrogen peroxide) during the first three hours. The NRF2 pathway is known to protect cells from hydrogen peroxide by reducing its levels [32]. For the nanomolar concentration of F1, a sustained increase in proliferation was observed within three days, apparently related to a sustained inhibition of apoptosis. For the higher concentration, a proliferative effect and a simultaneous increase in apoptosis were observed in the first three hours, which later resulted in compensation for this excessive proliferation. As a hypothesis explaining this dual behavior, we can assume the induction of apoptosis due to an imbalance of $OO^{\cdot-}/H_2O_2$ associated with increased NRF2 activity with unchanged NOX4 activity. The ratio of these primary reactive oxygen species is crucial for cell life, and apoptosis can result from both an excess of hydrogen peroxide and a lack of it [33].

One day later, activation of NADPH oxidase 4 was evident. The NOX4 gene encoded the catalytic subunit of the NADPH-oxidase complex, which catalyzed the reduction of molecular oxygen to superoxide anion. This may be due to the compensatory in response to “antioxidative” stress. NOX4 regulates the NRF2 pathway [34], but NRF2 also regulates NOX4 expression. Thus, knockdown of NRF2 expression by miRNAs resulted in attenuation of NOX4 expression [35]. An increase in NOX4 expression after 1 to 3 days naturally led to oxidative DNA damage for both concentrations studied and an increase in apoptosis for the higher concentration of F1. We can hypothesize that it is the increased expression of this pro-oxidant enzyme that causes the later increase in intracellular ROS to the control level.

5. Conclusions

The main feature of this compound is the ability to affect the intracellular metabolism of ROS through an ambiguous effect on the expression of key genes of the NRF2–NOX4 system. During the first three hours, F1 derivative activated NRF2 expression, which led to a balance shift towards ROS deficiency and inhibition of apoptosis. After 24–72 h of cultivation of HELF in the presence of F1, increases in the NOX4 gene and NOX4 protein expression level were observed that may be a result of compensatory process. This resulted in active synthesis of ROS in cells and development of a “prolonged” damaging effect of compounds on cells, expressed as increased levels of oxidative modifications and DNA double-strand breaks of cell nuclei and increased apoptosis. In relation to the cell cycle, a multidirectional effect of low and high concentrations of the compound was shown. The cytotoxic effect was not characteristic for the low concentration, while the cytotoxic effect for the high concentration appeared after 24–72 h of cultivation. This phenomenon can be explained by the imbalance in primary reactive oxygen species associated with increased NRF2 activity with unchanged NOX4 activity.

Supplementary Materials: The following supporting information can be downloaded at: <https://www.mdpi.com/article/10.3390/oxygen3010001/s1>, Figure S1: Synthesis of water-soluble fullerene derivative F1 from chlorofullerene $C_{60}Cl_6$, Figure S2: DLS profile revealing particle size distribution in aqueous solutions of the fullerene derivative F1. Figure S3: The excitation spectrum of the F1 solution in the culture medium (1.5 μ M) (λ_{fl} = 620 nm) (a); the fluorescence spectra of F1 at λ_{ex} = 280 nm (b) and λ_{ex} = 370 nm (c). Figure S4: The absorption spectrum of the F1 solution in deionized water (1.5 μ M). Figure S5: MTT-test: the positive control with dimethyl sulfoxide (0.0001%–50%); a 96-well scheme (a) and the cell viability vs DMSO concentration (b) [25,36].

Author Contributions: Conceptualization, S.V.K. and E.V.P.; methodology, S.V.K. and E.V.P.; validation, S.V.K., E.V.P. and P.A.T.; investigation, E.A.S., T.A.S., O.A.K., L.V.K., E.M.M., I.V.R. and O.A.D.; resources, N.N.V.; data curation, S.V.K., E.V.P., P.A.T. and N.N.V.; writing—original draft preparation, S.V.K. and E.V.P.; writing—review and editing, S.V.K. and E.V.P.; visualization, N.N.V.; supervision, N.N.V.; project administration, N.N.V. and S.V.K.; funding acquisition, S.V.K. All authors have read and agreed to the published version of the manuscript.

Funding: Synthesis of the fullerene derivative and investigation of the expression of a number of genes and proteins were supported by the Russian Science Foundation (project 19-13-00411-P). The study of the fluorescent properties of the fullerene derivative was supported by a government assignment from the Ministry of Science and Higher Education. Investigation of cytotoxicity and antioxidant properties of the fullerene was supported by the Russian Science Foundation (project 18-15-00437-P).

Institutional Review Board Statement: Not applicable.

Informed Consent Statement: Not applicable.

Data Availability Statement: All of the data is contained within the article and the supplementary materials.

Conflicts of Interest: The authors declare no conflict of interest.

References

1. Gaur, M.; Misra, C.; Yadav, A.B.; Swaroop, S.; Maolmhuaidh, F.O.; Bechelany, M.; Barhoum, A. Biomedical Applications of Carbon Nanomaterials: Fullerenes, Quantum Dots, Nanotubes, Nanofibers, and Graphene. *Materials* **2021**, *14*, 5978. [CrossRef] [PubMed]
2. Chistyakov, V.A.; Smirnova, Y.O.; Prazdnova, E.V.; Soldatov, A.V. Possible mechanisms of fullerene C(6)(0) antioxidant action. *BioMed Res. Int.* **2013**, *2013*, 821498. [CrossRef] [PubMed]
3. Markovic, Z.; Trajkovic, V. Biomedical potential of the reactive oxygen species generation and quenching by fullerenes (C₆₀). *Biomaterials* **2008**, *29*, 3561–3573. [CrossRef] [PubMed]
4. Kraevaya, O.A.; Novikov, A.V.; Shestakov, A.F.; Ershova, E.S.; Savinova, E.A.; Kameneva, L.V.; Veiko, N.N.; Schols, D.; Balzarini, J.; Kostyuk, S.V.; et al. Water-soluble fullerene-based nanostructures with promising antiviral and myogenic activity. *Chem. Commun.* **2020**, *56*, 10203–10206. [CrossRef]
5. Li, T.; Dorn, H.C. Biomedical Applications of Metal-Encapsulated Fullerene Nanoparticles. *Small* **2017**, *13*, 1603152. [CrossRef]
6. Huang, J.; Zhou, C.; He, J.; Hu, Z.; Guan, W.C.; Liu, S.H. Protective effect of reduced glutathione C₆₀ derivative against hydrogen peroxide-induced apoptosis in HEK 293T cells. *J. Huazhong Univ. Sci. Technol. Med. Sci.* **2016**, *36*, 356–363. [CrossRef]
7. Sergeeva, V.; Kraevaya, O.; Ershova, E.; Kameneva, L.; Malinovskaya, E.; Dolgikh, O.; Konkova, M.; Voronov, I.; Zhilenkov, A.; Veiko, N.; et al. Antioxidant Properties of Fullerene Derivatives Depend on Their Chemical Structure: A Study of Two Fullerene Derivatives on HELFs. *Oxid. Med. Cell. Longev.* **2019**, *2019*, 4398695. [CrossRef]
8. Troshina, O.A.; Troshin, P.A.; Peregudov, A.S.; Kozlovskiy, V.I.; Balzarini, J.; Lyubovskaya, R.N. Chlorofullerene C₆₀Cl₆: A precursor for straightforward preparation of highly water-soluble polycarboxylic fullerene derivatives active against HIV. *Org. Biomol. Chem.* **2007**, *5*, 2783–2791. [CrossRef]
9. Kornev, A.B.; Khakina, E.A.; Troyanov, S.I.; Kushch, A.A.; Peregudov, A.; Vasilchenko, A.; Deryabin, D.G.; Martynenko, V.M.; Troshin, P.A. Facile preparation of amine and amino acid adducts of [60]fullerene using chlorofullerene C₆₀Cl₆ as a precursor. *Chem. Commun.* **2012**, *48*, 5461–5463. [CrossRef]
10. Khakina, E.A.; Kraevaya, O.A.; Popova, M.L.; Peregudov, A.S.; Troyanov, S.I.; Chernyak, A.V.; Martynenko, V.M.; Kulikov, A.V.; Schols, D.; Troshin, P.A. Synthesis of different types of alkoxy fullerene derivatives from chlorofullerene C₆₀Cl₆. *Org. Biomol. Chem.* **2017**, *15*, 773–777. [CrossRef]
11. Yoshioka, W.; Tohyama, C. Mechanisms of Developmental Toxicity of Dioxins and Related Compounds. *Int. J. Mol. Sci.* **2019**, *20*, 617. [CrossRef] [PubMed]
12. Katagiri, T.; Takeuchi, T.; Mine, T.; Noguchi, T.; Nishizawa, T.; Yamamoto, S.; Okudaira, M.; Matsushima, T. Chronic inhalation toxicity and carcinogenicity studies of 3-chloro-2-methylpropene in BDF1 mice. *Ind. Health* **2000**, *38*, 309–318. [CrossRef] [PubMed]
13. Valentovic, M.A.; Ball, J.G.; Hong, S.K.; Rogers, B.A.; Meadows, M.K.; Harmon, R.C.; Rankin, G.O. In Vitro toxicity of 2- and 4-chloroaniline: Comparisons with 4-amino-3-chlorophenol, 2-amino-5-chlorophenol and aminophenols. *Toxicol. In Vitro* **1996**, *10*, 713–720. [CrossRef] [PubMed]
14. Schweigert, N.; Hunziker, R.W.; Escher, B.I.; Eggen, R.I. Acute toxicity of (chloro-)catechols and (chloro-)catechol-copper combinations in *Escherichia coli* corresponds to their membrane toxicity in vitro. *Environ. Toxicol. Chem.* **2001**, *20*, 239–247. [CrossRef]
15. Zhang, T.; Li, X.; Min, X.; Fang, T.; Zhang, Z.; Yang, L.; Liu, P. Acute toxicity of chlorobenzenes in tetrahymena: Estimated by microcalorimetry and mechanism. *Environ. Toxicol. Pharmacol.* **2012**, *33*, 377–385. [CrossRef] [PubMed]
16. Yin, J.; Wu, B.; Zhang, X.X.; Xian, Q. Comparative toxicity of chloro- and bromo-nitromethanes in mice based on a metabolomic method. *Chemosphere* **2017**, *185*, 20–28. [CrossRef]
17. Wang, J.; Zhang, H.; Zheng, X.; Liu, R.; Zong, W. In vitro toxicity and molecular interacting mechanisms of chloroacetic acid to catalase. *Ecotoxicol. Environ. Saf.* **2020**, *189*, 109981. [CrossRef] [PubMed]
18. Sies, H. Oxidative stress: Oxidants and antioxidants. *Exp. Physiol.* **1997**, *82*, 291–295. [CrossRef]
19. Lambeth, J.D.; Neish, A.S. Nox enzymes and new thinking on reactive oxygen: A double-edged sword revisited. *Annu. Rev. Pathol.* **2014**, *9*, 119–145. [CrossRef]
20. Sies, H. Total antioxidant capacity: Appraisal of a concept. *J. Nutr.* **2007**, *137*, 1493–1495. [CrossRef]

21. Martin, K.R.; Barrett, J.C. Reactive oxygen species as double-edged swords in cellular processes: Low-dose cell signaling versus high-dose toxicity. *Hum. Exp. Toxicol.* **2002**, *21*, 71–75. [[CrossRef](#)] [[PubMed](#)]
22. Pan, J.S.; Hong, M.Z.; Ren, J.L. Reactive oxygen species: A double-edged sword in oncogenesis. *World J. Gastroenterol.* **2009**, *15*, 1702–1707. [[CrossRef](#)] [[PubMed](#)]
23. Ferrer, M.D.; Sureda, A.; Mestre, A.; Tur, J.A.; Pons, A. The double edge of reactive oxygen species as damaging and signaling molecules in HL60 cell culture. *Cell. Physiol. Biochem.* **2010**, *25*, 241–252. [[CrossRef](#)]
24. Mijatovic, S.; Savic-Radojevic, A.; Pljesa-Ercegovic, M.; Simic, T.; Nicoletti, F.; Maksimovic-Ivanic, D. The Double-Faced Role of Nitric Oxide and Reactive Oxygen Species in Solid Tumors. *Antioxidants* **2020**, *9*, 374. [[CrossRef](#)] [[PubMed](#)]
25. Kraevaya, O.A.; Peregudov, A.S.; Troyanov, S.I.; Godovikov, I.; Fedorova, N.E.; Klimova, R.R.; Sergeeva, V.A.; Kameneva, L.V.; Ershova, E.S.; Martynenko, V.M.; et al. Diversion of the Arbusov reaction: Alkylation of C-Cl instead of phosphonic ester formation on the fullerene cage. *Org. Biomol. Chem.* **2019**, *17*, 7155–7160. [[CrossRef](#)]
26. Ershova, E.S.; Sergeeva, V.A.; Chausheva, A.I.; Zheglo, D.G.; Nikitina, V.A.; Smirnova, T.D.; Kameneva, L.V.; Porokhovnik, L.N.; Kutsev, S.I.; Troshin, P.A.; et al. Toxic and DNA damaging effects of a functionalized fullerene in human embryonic lung fibroblasts. *Mutat. Res. Genet. Toxicol. Environ. Mutagen.* **2016**, *805*, 46–57. [[CrossRef](#)] [[PubMed](#)]
27. Ershova, E.S.; Sergeeva, V.A.; Tabakov, V.J.; Kameneva, L.A.; Porokhovnik, L.N.; Voronov, I.I.; Khakina, E.A.; Troshin, P.A.; Kutsev, S.I.; Veiko, N.N.; et al. Functionalized Fullerene Increases NF-kappaB Activity and Blocks Genotoxic Effect of Oxidative Stress in Serum-Starving Human Embryo Lung Diploid Fibroblasts. *Oxid. Med. Cell. Longev.* **2016**, *2016*, 9895245. [[CrossRef](#)]
28. Itoh, K.; Wakabayashi, N.; Katoh, Y.; Ishii, T.; Igarashi, K.; Engel, J.D.; Yamamoto, M. Keap1 represses nuclear activation of antioxidant responsive elements by Nrf2 through binding to the amino-terminal Neh2 domain. *Genes Dev.* **1999**, *13*, 76–86. [[CrossRef](#)]
29. Yamamoto, T.; Suzuki, T.; Kobayashi, A.; Wakabayashi, J.; Maher, J.; Motohashi, H.; Yamamoto, M. Physiological significance of reactive cysteine residues of Keap1 in determining Nrf2 activity. *Mol. Cell. Biol.* **2008**, *28*, 2758–2770. [[CrossRef](#)]
30. Poljsak, B.; Milisav, I. The neglected significance of “antioxidative stress”. *Oxid. Med. Cell. Longev.* **2012**, *2012*, 480895. [[CrossRef](#)]
31. Gandhi, V.V.; Phadnis, P.P.; Kunwar, A. 2,2'-Dipyridyl diselenide (Py2Se2) induces G1 arrest and apoptosis in human lung carcinoma (A549) cells through ROS scavenging and reductive stress. *Metallomics* **2020**, *12*, 1253–1266. [[CrossRef](#)] [[PubMed](#)]
32. Ma, T.J.; Lan, D.H.; He, S.Z.; Ye, Z.; Li, P.; Zhai, W.; Chen, W.Q.; Huang, Y.; Fu, Y.; Sun, A.; et al. Nrf2 protects human lens epithelial cells against H2O2-induced oxidative and ER stress: The ATF4 may be involved. *Exp. Eye Res.* **2018**, *169*, 28–37. [[CrossRef](#)] [[PubMed](#)]
33. Pervaiz, S.; Clement, M.V. Hydrogen peroxide-induced apoptosis: Oxidative or reductive stress? *Methods Enzymol.* **2002**, *352*, 150–159. [[CrossRef](#)] [[PubMed](#)]
34. Brewer, A.C.; Mustafi, S.B.; Murray, T.V.; Rajasekaran, N.S.; Benjamin, I.J. Reductive stress linked to small HSPs, G6PD, and Nrf2 pathways in heart disease. *Antioxid. Redox Signal.* **2013**, *18*, 1114–1127. [[CrossRef](#)] [[PubMed](#)]
35. Pendyala, S.; Moitra, J.; Kalari, S.; Kleeberger, S.R.; Zhao, Y.; Reddy, S.P.; Garcia, J.G.; Natarajan, V. Nrf2 regulates hyperoxia-induced Nox4 expression in human lung endothelium: Identification of functional antioxidant response elements on the Nox4 promoter. *Free Radic. Biol. Med.* **2011**, *50*, 1749–1759. [[CrossRef](#)]
36. Troshin, P.A.; Popkov, O.; Lyubovskaya, R.N. Some New Aspects of Chlorination of Fullerenes. *Fuller. Nanotub. Carbon Nanostruct.* **2003**, *11*, 165–185. [[CrossRef](#)]

Disclaimer/Publisher’s Note: The statements, opinions and data contained in all publications are solely those of the individual author(s) and contributor(s) and not of MDPI and/or the editor(s). MDPI and/or the editor(s) disclaim responsibility for any injury to people or property resulting from any ideas, methods, instructions or products referred to in the content.